**Total reaction cross section measurement and neutron density distribution in light stable and radioactive nuclei**

R. Wada, W. Lin, P. Ren, I. Tanihata, and D.T. Tran

This experimental study aims to determine the neutron density distribution in light isotopes, especially very neutron rich isotopes. Such data would provide a mean not only to distinguish skin type and hallo type nuclei, but also enable to extract the parameters of their neutron density distribution.

Neutron density distribution of light exotic nuclei has been studied experimentally and theoretically in the last 30 years using total reaction cross section (TRCS) measurements. However, there are still large uncertainties, because the contributions from the halo or skin of neutron distributions in TRCS are rather small, and in order to eliminate such ambiguities, precise measurements with accuracy of an order of 1% are necessary.

The basic idea of this study based on the fact that the contribution of the nuclear matter distribution to TRCS depends on the incident energy. In order to illustrate this, we performed simple calculations, using the Glauber model. Fig. 1 shows the calculated ratios of TRCS of hypothetical skin- or

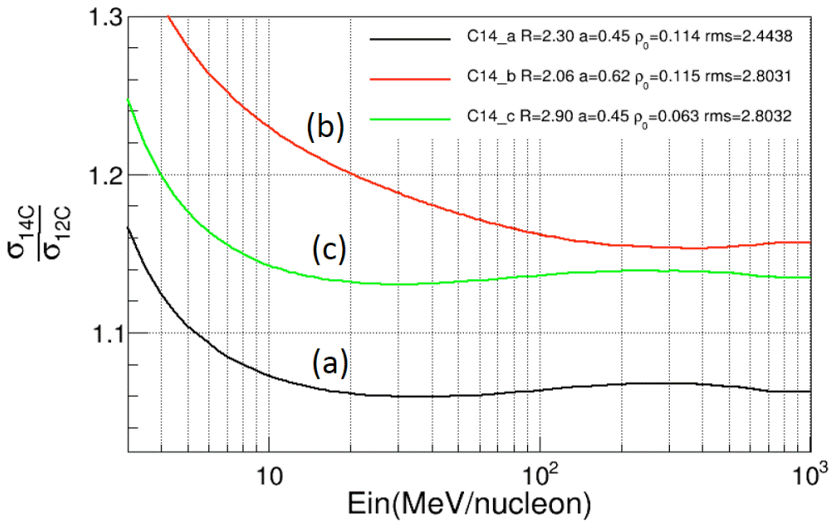


**FIG. 1.** Calculated ratios of the total reaction cross section of hypothetical skin- or halo-type $^{14}$C nucleus relative to that of $^{12}$C are shown as a function of the incident energy.

halo-type $^{14}$C nucleus relative to that of $^{12}$C are shown as a function of the incident beam energy. When we use the same diffuseness parameter for $^{14}$C (we call it a skin type $^{14}$C) as $^{12}$C, the ratio stays flat from 10 – 1000 MeV/nucleon range. In Fig. 1, line (a) and line (b) show the absolute cross section increase in proportional to the RMS radius. On the other hand when we use a halo-type $^{14}$C with a larger diffuseness, then the ratio starts to increase below 100 MeV/nucleon as shown in line (c). This is because, at high energy regime, the total reaction cross section is determined mainly by the nuclear interaction near the

surface around the RMS radius, but at lower energy regime, the neutron distribution at large radius makes a notable contribution to TRCS because of nucleon-nucleon collisions. This exercise indicates that if one can measure the excitation function of TRCS below 100 MeV/nucleon with a sufficient accuracy, one can determine the neutron density distribution at larger radius experimentally. One should note that the increment of the TRCS at 100 MeV/nucleon and at 20 MeV/nucleon is an order of 5 % or less. Therefore in order to distinguish the differences, the accuracy of an order of 1 % is necessary for the TRCS measurements.

The first experiment was performed in 2014 at RCNP, Osaka University, in Japan, using the secondary beams. $^{22}$Ne beam were bombarded on $^{9}$Be target at F0 at 80 A MeV. The generated secondary beams were delivered to the detector system shown in Fig.2, using two dipole magnets between F1-F2 and F2-F3. The isotope identification of the incident isotopes before the target is performed by three time of flight measurements between PPACS and plastic detector and the energy loss in the Si detector right before the target. The identification of the isotopes after the target is made by MUSIC (MUlti-Sampling Ionization Chamber) and the energy is measured by NaI. MUSIC detector was used in order to avoid the channeling effect in Si detector, which often caused significant background for the isotope identification.

Typical particle identifications before the target and after the target are shown in Fig.3. TRCS. $\sigma_R$,

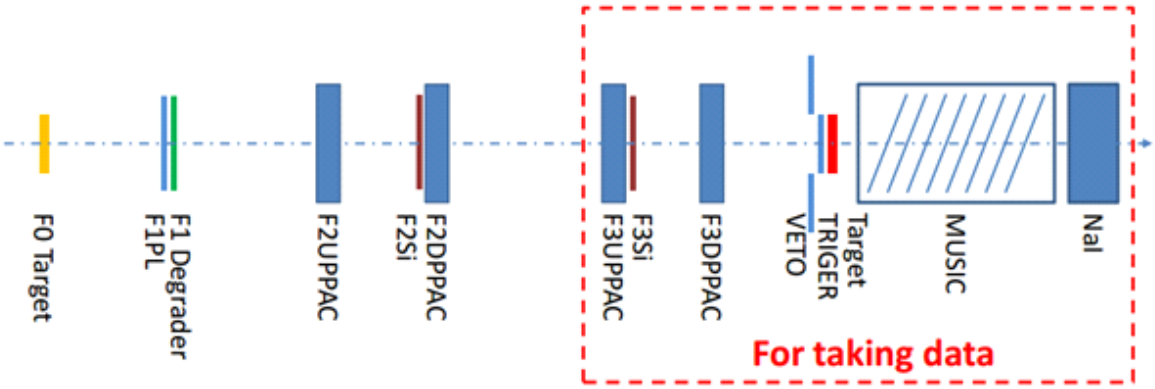


**FIG. 2.** Schematic view of the beam line and detector system.

is calculated by the following formula,

$$\sigma_R = \frac{1}{t} ln \left[ \frac{\gamma_0 (1 - P_{m0})}{\gamma (1 - P_m)} \right]$$

$\gamma = N_{out}/N_{in}$ is with the target and $\gamma_0$ is that without the target. N is the number of isotope before the target (in) and after the target (out). t is the target thickness. $P_m$ *and* $P_{m0}$ are the correction factors for the inelastic scattering loss in the target and the elastic loss in the MUSIC chamber.

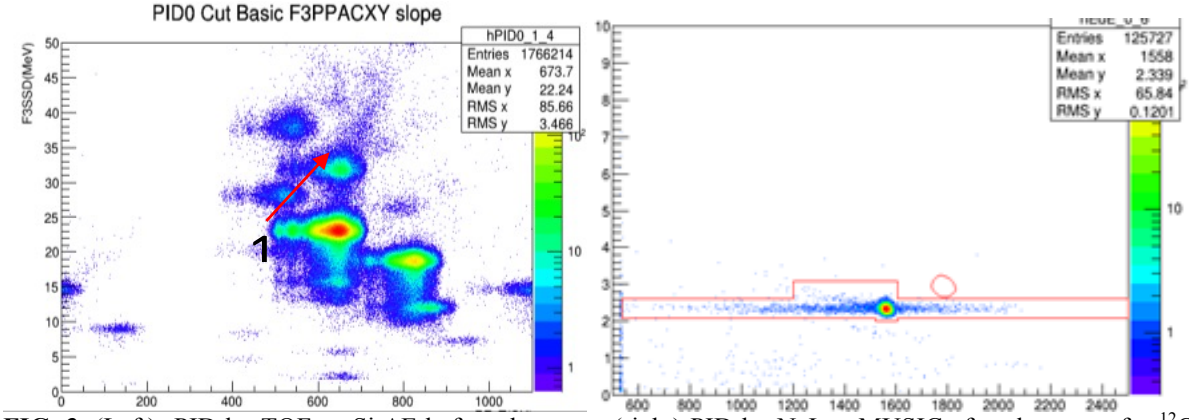


**FIG. 3.** (Left) PID by TOF vs Si-ΔE before the target (right) PID by NaI vs MUSIC after the target for $^{12}$C run.

The inelastic loss is evaluated by comparing the NaI energy spectra with and without the target runs as shown in the left panel of Fig.4. Blue histogram is the spectra with target and red one is without. Both spectra are normalize at the elastic peak. On the right the elastic loss is evaluated using 8 segments of the MUSIC chamber and NaI. ΔN is the counts difference between the two consecutive segments in the MUSIC chamber. The highest yield at ~ 5$^{o}$ is the difference between the last segment of MUSIC and NaI. The red curve is the predicted yields from the Rutherford (Mott) scattering. Further data analysis is underway.

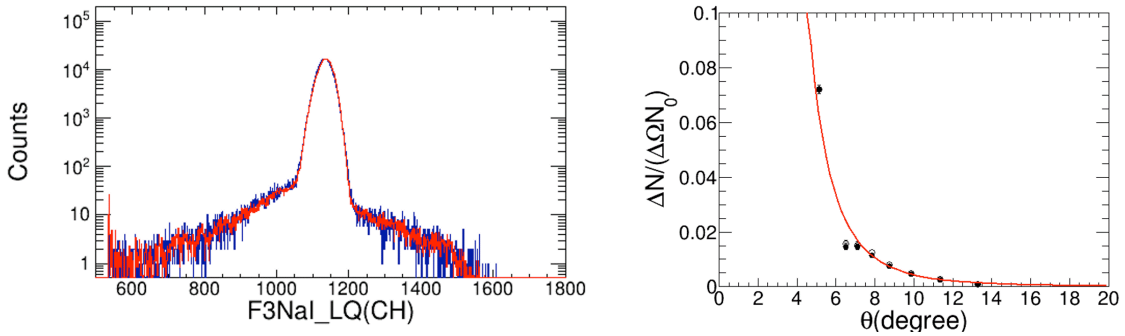


**FIG. 4.** (Left) Energy spectra with (blue) and without (red) target runs for *Pm* correction. (Right) Elastic scattering loss in the MUSIC chamber and NaI after the target for *Pm0* correction. Both are from $^{12}$C run.